Extraction of Distribution Function of Relaxation Times by using DRT-RBLM Tools: A New Approach to Combine Levenberg-Marquardt Algorithm and Radial Basis Functions for Discretization Basis

Journal of The Electrochemical Society, 2022 **169** 110529
1945-7111/2022/169(11)/110529/12/$40.00 © 2022 The Electrochemical Society ("ECS"). Published on behalf of ECS by IOP Publishing Limited

Extraction of Distribution Function of Relaxation Times by using DRT-RBLM Tools: A New Approach to Combine Levenberg-Marquardt Algorithm and Radial Basis Functions for Discretization Basis

M. Kunaver,[1] Ž. Rojec,[1] V. Subotić,[2] S. Pereverzyev,[3] and M. Žic[4,z]

[1]*Faculty of Electrical Engineering, University of Ljubljana, 1000 Ljubljana, Slovenia*
[2]*Institute of Thermal Engineering, Graz University of Technology, 8010 Graz, Austria*
[3]*Johann Radon Institute for Computational and Applied Mathematics, A-4040 Linz, Austria*
[4]*Ruđer Bošković Institute, 10000 Zagreb, Croatia*

Electrochemical Impedance Spectroscopy (EIS) is a powerful tool for the analysis of different power sources and various materials. One of the methods used for studying EIS data is the distribution function of relaxation times (DRT). EIS data can be converted into a Fredholm integral of the first kind; and DRT extraction is known to be an inverse ill-posed problem. Herein, a new strategy to extract DRT by applying the Levenberg-Marquardt algorithm (LMA) is proposed. The Jacobian matrix appearing in LMA is partially numerically approximated by applying the radial basis function as a basis for the discretization. DRT data are smoothed by the application of the finite difference matrix and the negative values are avoided by the limits application. The tests conducted with ZARCs/FRACs synthetic data show that the extracted DRT profiles correspond well to their analytical counterparts. The application of LMA in solving Fredholm integral equation of the first kind (i.e., DRT extraction) resulted in the automatic tuning of the regularization parameter. The aforementioned findings show that by modifying LMA it is possible to both solve the Fredholm integral equation of the first kind in a completely data-driven way and to obtain the applicable DRT data for general EIS study.
 [DOI: 10.1149/1945-7111/ac9a83]

Manuscript submitted June 13, 2022; revised manuscript received September 14, 2022. Published November 16, 2022.

List of Symbols

b	experimental or synthetic data
y	simulated data obtained by some model Y
Y	arbitrary mathematical model
K	number of ZARC (and FRAC) elements
$\vec{Z}_{data}$	measured impedance data
ω	angular frequency
f	frequency
τ	time constant
$G(ln\ \tau)$	distribution function of relaxation times in log scale
$g(\tau)$	distribution function of relaxation times
N	number of impedance data points
DRT	distribution function of relaxation times
γ	characteristic of $g(\tau)$
$\vec{\gamma}$	parameter vector containing γ_j
$\mathbf{Z}^{Re}$	matrix representing $\frac{\partial \mathrm{Re}(\vec{Z}_{model})}{\partial \gamma}$
$\mathbf{Z}^{Im}$	matrix representing $\frac{\partial \mathrm{Im}(\vec{Z}_{model})}{\partial \gamma}$
$\mathbf{J}$	Jacobian matrix
$\mathbf{W}$	diagonal matrix containing weights ($W_{j,j} = 1$)
$\vec{\delta}$	vector of computed increment
l	iteration number
FWHM	full width at the half maximum
ϵ	RBF shape parameter
ϵ_1	convergence tolerance in the gradient
ϵ_2	convergence tolerance in the parameter value
LMA	Levenberg-Marquardt algorithm
FRAC	impedance data obtained by Davison-Cole model
Z_{ZARCs}	synthetic ZARCs impedance data
Z_{FRACs}	synthetic FRACs impedance data
R	resistor
L	inductance
i	imaginary unit
$\mathrm{DRT}_{\mathrm{ZARCs}}$	DRT extracted from ZARCs data
$\mathrm{DRT}_{\mathrm{FRACs}}$	DRT extracted from FRACs data
Z_{poll}	polluted synthetic ZARCs (or FRACs) EIS data
NF	noise factor
η'	normally distributed random variable with zero mean and the variance one
η''	normally distributed random variable with zero mean and the variance one
$\vec{r}$	residual ($\vec{Z}_{data} - \vec{Z}_{model}(\gamma)$) and ($b - y$)
$\mathbf{J}^T\mathbf{W}\vec{r}$	gradient vector
$\mathbf{J}^T\mathbf{W}\mathbf{J}$	approximated Hessian matrix
$\mathbf{Q}$	smoothing operator
λ	"damping" factor
Z_{model}	matrix model that generates impedance data
n	parameter related to constant phase element
RNTM	a reflective Newton type method
$\mathbf{H}$	column vector with components $H_j = \omega_j$.

Electrochemical impedance spectroscopy.—Electrochemical Impedance Spectroscopy (EIS) has become a very popular experimental technique to diagnose electrical systems and different power sources. EIS data can be represented as

$$\vec{Z}_{data} = (Z_{data,1}, Z_{data,2},\ldots,Z_{data,N}), \qquad [1]$$

consisting of impedance measurements $Z_{data,j} = Z^{Re}_{data,j} + iZ^{Im}_{data,j}$ collected at different collocation points, i.e., at different angular frequencies ω_j, $j = 1, 2,\ldots,N$, where N is the number of acquired EIS data points.

EIS data can also be expressed in the form of the Fredholm integral[1] of the first kind:

$$Z(\omega_j) = \int_0^\infty \frac{g(\tau)}{1 + i\omega_j\tau}\, d\tau, \qquad [2]$$

where τ and $g(\tau)$ are the time constant and non-negative Distribution of the Relaxation Times (DRT). DRT is of significant interest in EIS studies as it enables a model-free approach to analyze EIS data.[2] Furthermore, extraction of $g(\tau)$ from 2 is a classic inverse ill-posed problem that has to be attacked by various mathematical techniques.[1]

One of the general problems in the DRT topic is the choice of the numerical method. The majority of DRT approaches apply

[z]E-mail: mzic@irb.hr

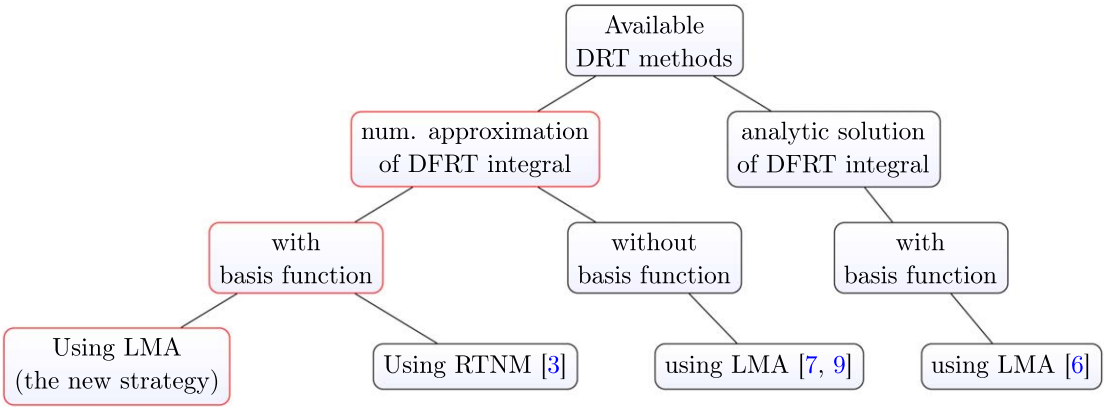

Scheme 1. Schematic representation of selected DRT strategies (and their simplified workflows) that are of keen interest in this work. The workflow marked in red represents a new avenue of research (i.e., the proposed new strategy) that has not been reported in DRT studies yet.

regularization,[1] but then it is necessary to choose the regularization parameter. This parameter can be manually given,[3,4] obtained by cross-validation[3] and self-consistent techniques,[5] and automatically tuned.[2,6] Also, the DRT extraction is an inverse ill-posed problem; and thus, DRT is prone to oscillations.

It is common to acquire and display EIS measurements on a logarithmic scale; and thus, the following substitutions $\tau = e^y$ and $d\tau = e^y dy$ can be applied:

$$Z(\omega_j) = \int_{-\infty}^{\infty} \frac{g(e^y)}{1 + i\omega_j e^y} e^y dy = \int_{-\infty}^{\infty} \frac{G(y)}{1 + i\omega_j e^y} dy, \quad [3]$$

where $g(e^y)e^y$ is equal to $G(y)$. Please note that the integral in 3 is suitable for numerical integration in the logarithmic scale.

Furthermore, if $y = ln\ \tau$, $dy = d\ ln\ \tau$ and $e^y = e^{ln\ \tau} = \tau$, then we can rewrite 3 as follows:

$$Z(\omega_j) = \int_{-\infty}^{\infty} \frac{G(ln\ \tau)}{1 + i\omega_j \tau}\ d\ ln\ \tau, \quad [4]$$

where the real and imaginary components of 4 are:

$$Z(\omega_j) = \int_{-\infty}^{\infty} \frac{G(ln\ \tau)}{1 + \omega_j^2 \tau^2} d\ ln\ \tau + i \int_{-\infty}^{\infty} \frac{\omega_j \tau G(ln\ \tau)}{1 + \omega_j^2 \tau^2}\ d\ ln\ \tau. \quad [5]$$

Since the DRT deconvolution is an inverse ill-posed problem, it is advisable to apply different extraction approaches, e.g.,[3,6,7] in order to conduct a model-free EIS study.

Methods to extract distribution function of relaxation times.—The available strategies for DRT extraction are based on regularization techniques,[2,3,6–9,4] Fourier filtering,[10,11] evolutionary programming[12–14] grammatical evolution,[15] maximum entropy model,[16] Monte Carlo techniques,[17] deconvolution using deep neural networks[18] and Finite Gaussian Processes.[19,20] Interestingly enough, only a few of the listed aforementioned regularization approaches apply the Levenberg-Marquardt algorithm (LMA) to extract the applicable DRT profiles from EIS data.[6,7,9] Herein, we are focused on both the LMA regularization and on the Jacobian matrix approximation; and thus, we have revisited several DRT strategies[3,6,7,9] that are of keen interest (Scheme 1).

In our previous study,[6] we applied the analytical solution of the integral in 2 as a part of the Jacobian matrix, which allowed the extraction of the applicable DRT profile by LMA (Scheme 1). However, as explained in Ref. 6, the extracted DRT profiles were not always positive, which generally hinders EIS analyzes. Oppositely, the positive and bell-shaped DRT profiles were reported by Wan et al.,[3] since the authors applied the radial basis function (RBF) as a basis for discretization (Scheme 1). RBFs are especially suitable for DRT study as they are symmetrical and their shape is governed by both the distance from the center and the shape factor.

Wan et al.[3] extracted positive and bell-shaped DRT profiles by applying both RBFs and a reflective Newton type method (RNTM) for minimizing a quadratic functions of many variables.[21] The aforementioned combination in turn yielded smooth and positive DRT profiles. However, RNTM has to solve an additional subproblem(s) which is a demanding computation task. Therefore, to ensure the positive and bell-shaped DRT profiles and to facilitate computing tasks in this work, the following actions were taken. First, to secure bell-shaped DRT profiles, the integral in 4 was numerically approximated by using RBF as a basis for discretization (see Ref. 3). Second, to avoid additional subproblem solving, we have utilized the "damped" LMA version.[22,23] And finally, the "damped" LMA was modified with intention to produce smooth and positive DRT values, a task which has not been reported in DRT study yet.

The aim of this work is to develop and justify a new strategy that yields both smooth and positive DRT profiles by using a simpler LMA (vs RNTM) method (Scheme 1). In the following sections, we will briefly revisit[3] the theory behind the numerical approximation of the integral in 4 by using RBF as a basis for discretization. Moreover, the general DRT model will be explained and an approach to form the Jacobian matrix will be offered. Consequently, we will explain LMA in detail and propose strategies to obtain smooth and positive DRT profiles. According to the aforementioned analyses supported by the literature,[3,6,7,9] it follows that our idea actually represents a new avenue of research (Scheme 1). And finally, a newly designed strategy will be tested by analyzing various synthetic ZARCs and FRACs data.

Theory

Numerical discretization by application of radial basis function as a basis for discretization.—The literature offers a various straightforward approaches to numerically discretize the integral 2 and one of them was utilized by both Risse et al.[24] and Kulikovsky.[7] The authors applied LMA and the right rectangular quadrature rule to discretize the integral in 2, but without the application of the basis functions for discretization. However, according to Wan et al.,[3] the integral in 4 can be discretized by the utilization of the radial basis function(s) (RBFs) as the basis for discretization. The RBF application is favored in EIS study as it smooths DRT data and, at the same time, it decreases discretization errors. However, this does not come

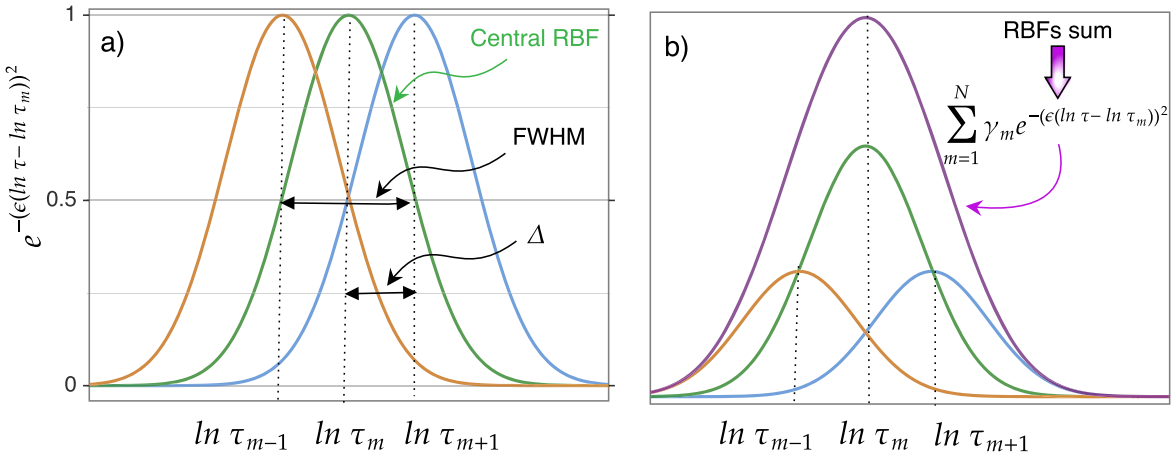

Scheme 2. Schematic presentation of (a) the bell-shaped Gaussian curves (RBFs) and (b) their sum. Subplot (a) shows FWHM (of the central RBF) which was set equal to 2Δ. Subplot (b) displays the positive RBFs sum obtained due to the application of arbitrarily chosen $\vec{\gamma} > 0$ values. Scheme is inspired by Ref. 3.

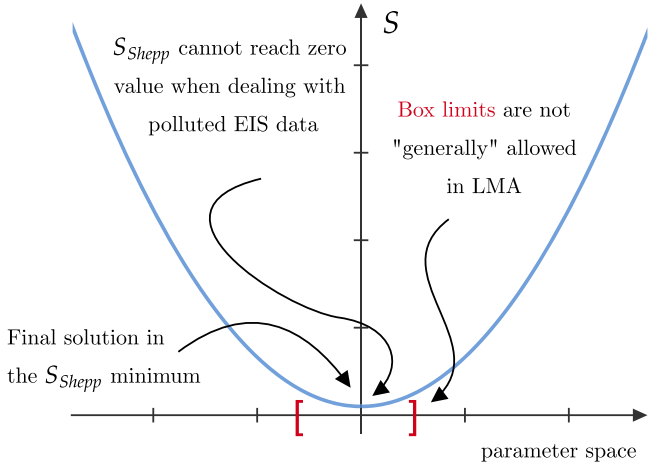

Scheme 3. Schematic representation of S_{Shepp} function. The application of limits is also commented on. The zero value cannot be reached when applying polluted EIS data.

without a cost; namely, due to the RBF application in this work, the analytical solution of the integral in 4 is not available. Thus, the application of both LMA and RBF in this work distinguishes the proposed strategy (Scheme 1b) from the ones reported in the literature.[3,7,9] The following analyses concerning the RBF application in DRT study follow the work by Wan et al.[3] and their online code.

In order to decrease the discretization errors, $G(\tau)$ in 4 can be approximated by a sum of bell-shaped functions (ϕ) at the collocation points $\tau_1, \tau_2, \ldots\tau_m$:

$$G(ln\ \tau) = \sum_{m=1}^{m=N} \gamma_m \phi(|\, ln\ \tau - ln\ \tau_m|), \qquad [6]$$

where $\phi(x) = e^{-(\epsilon x)^2}$ is the Gaussian (Scheme 2a) and ϵ is the shape parameter.

The full width at the half maximum (FWHM) of the Gaussian can be explicitly expressed in the terms of ϵ, i.e., FWHM $= (ln2)^{1/2}/\epsilon$. However, in this work, FWHM was set by design to be equal to 2Δ(Scheme 2a); and consequently, ϵ was computed by using the following relation:[3]

$$\text{FWHM} = 2\Delta = \frac{(ln2)^{1/2}}{\epsilon} = \frac{1.665}{\epsilon}, \qquad [7]$$

where Δ represents the distance between $ln\ \tau_{m+1}$ and $ln\ \tau_m$. As ϵ takes larger values, DRT will oscillate more; and thus, ϵ should be addressed as an additional regularization parameter to DRT problem. Furthermore, Scheme 2b evidently demonstrates that the sum of RBFs 6 has the bell-shaped profile, a feature that is not easily obtained by using the basis function applied in our previous work (see Scheme 2 in Ref. 6). However, in contrast to this work, the

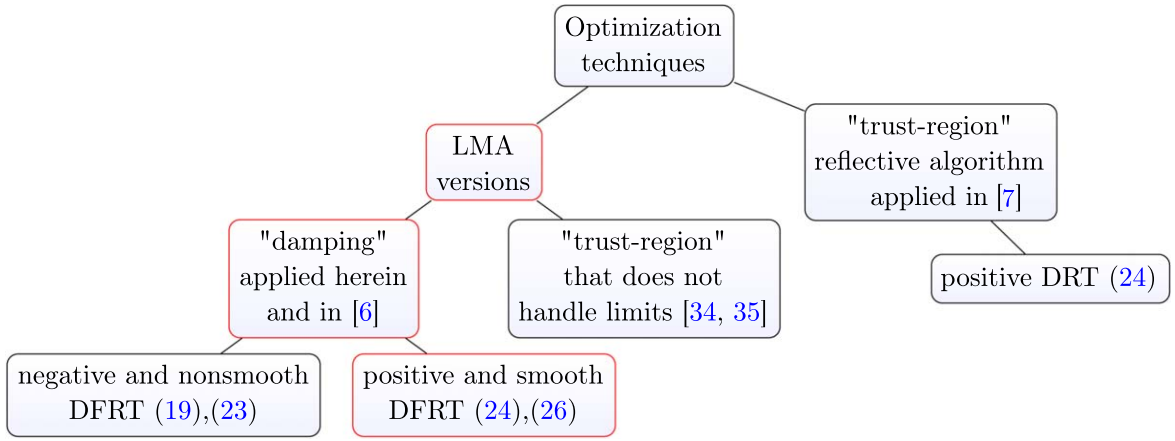

Scheme 4. Schematic representation of selected optimization techniques of keen interest utilized in DRT studies. The workflow marked in red represents a new avenue of research (i.e., the proposed strategy) that has not been reported in DRT study yet.

application of the basis function in Ref. 6 allowed us to analytically solve the integral in 2.

Next, by combining 5, 6, and by taking $y = ln\tau - ln\tau_m$, $dy = d\ ln\tau$, $\tau = e^y\tau_m$ and $\omega_j = 2\pi f_j$ we obtain the following expression:

$$Z(f_j) = \sum_{m=1}^{N} \gamma_m \left(\int_{-\infty}^{\infty} \frac{1}{1 + (2\pi f_j e^y \tau_m)^2} \phi(|y|) dy + i \int_{-\infty}^{\infty} \frac{2\pi f_j e^y \tau_m}{1 + (2\pi f_j e^y \tau_m)^2} \phi(|y|) dy \right), \quad [8]$$

where f_j is the frequency related to jth EIS data point. 8 can also be rewritten in the following matrix form:

$$Z(f_j) = \sum_{m=1}^{N} (A_{j,m}^{Re}\gamma_m + iA_{j,m}^{Im}\gamma_m). \quad [9]$$

Subsequently, if we take $f_j e^y \tau_m = f_j e^y f_m^{-1} = e^{lnf_j} e^y e^{-lnf_m} = e^{y+lnf_j-lnf_m}$, then the matrices $\mathbf{A}^{Re}$ and $\mathbf{A}^{Im}$ in 9 can be expressed as:[3]

$$A_{j,m}^{Re} = \int_{-\infty}^{\infty} \frac{1}{1 + 4\pi^2 e^{2(y+lnf_j-lnf_m)}} \phi(|y|)\ dy, \quad [10]$$

$$A_{j,m}^{Im} = \int_{-\infty}^{\infty} \frac{2\pi e^{y+lnf_j-lnf_m}}{1 + 4\pi^2 e^{2(y+lnf_j-lnf_m)}} \phi(|y|)\ dy. \quad [11]$$

Formulations 10, 11 can be used to form matrices $\mathbf{A}^{Re}$ and $\mathbf{A}^{Im}$ by applying the numerical integration technique(s) that is available in, e.g., SciPy.[25] At this point, it should be stressed that matrices $\mathbf{A}^{Re}$ and $\mathbf{A}^{Im}$ 10, 11 have not been used in LMA as part of the Jacobian matrix for DRT deconvolution yet.

General DRT model.—According to Refs. 3, 6, 9, 24, a more general impedance model can be given as:

$$Z_{model}(\omega_j) = R_\infty + i\omega_j L + \int_0^{\infty} \frac{G(ln\ \tau)}{1 + i\omega_j\tau} d\ ln\ \tau, \quad [12]$$

where R_∞ and L are, accordingly, resistance at high frequency limit and inductance. In line with Refs. 6, 24, the model 12 can be represented by the following discrete version:

$$\vec{Z}_{model} = \mathbf{Z}^{Re}\vec{\gamma} + i\mathbf{Z}^{Im}\vec{\gamma}, \quad [13]$$

where $\mathbf{Z}^{Re}$, $\mathbf{Z}^{Im}$ are both $N \times N + 2$ matrices that do not depend on $\vec{\gamma}$, i.e., $\mathbf{Z}^{Re} = [\mathbf{1}\ \ \mathbf{0}\ \ \mathbf{A}^{Re}]$ and $\mathbf{Z}^{Im} = [\mathbf{0}\ \ \mathbf{H}\ \ -\mathbf{A}^{Im}]$. Please note that $\mathbf{0}$ and $\mathbf{1}$ are column vectors with elements equal to 0 and 1 and $\mathbf{H}$ is a column vector with components $H_j = \omega_j$. $\mathbf{A}^{Im}$ has a negative sign due to the fact that $Im(\vec{Z}_{model})$ values are negative.

Since $\frac{\partial \vec{Z}_{model}}{\partial \gamma} = \mathbf{Z}^{Re} + i\mathbf{Z}^{Im}$, the matrices $\mathbf{Z}^{Re}$ and $\mathbf{Z}^{Im}$ represent an approximate Jacobian matrix of the mapping $\vec{\gamma} \rightarrow \vec{Z}_{model}$. Oppositely to our previous work,[6] in which we have applied an analytical solution of the DRT integral, the Jacobian matrix in this study consists of elements that were obtained by the numerical approximation of the integral in 12 via application of RBF as basis for discretization. In the next sections, we briefly explain the LMA fundamentals and the role of the Jacobian matrix in this study.

Levenberg-Marquardt algorithm.— *General information.*—The Levenberq-Marquardt algorithm (LMA) is commonly used to solve nonlinear least squares (NLS) problems.[26] However, in the previous work[6] we demonstrated that LMA can be used to solve the linear inverse ill-posed DRT problem. Also, we explained that LMA is more suitable for DRT extraction than both Landweber iterations[27] and the conjugate gradient method.[28] Thus, LMA is a proper tool for DRT study which can be attributed to the fact that it has the self-adapting regularization parameter[23] and it is prone to diverse modification(s) as shown in Refs. 29, 30.

LMA became even more popular in data science due to the work by Moré et al.[31] What is more, the authors published a famous MINPACK optimization library that is written in FORTRAN.[32] However, Moré's library is based on "trust region" concept, which means that instead of adjusting λ regularization parameter, the algorithm controls the trust region radius by solving an additional subproblem. Furthermore, LMA is especially designed to fit some nonlinear model (Y) to the data by utilizing the following quadratic objective function (S):[22,23]

$$S(\vec{\gamma}) = \sum_{j=1}^{N} \left(\frac{b_j - Y(\vec{\gamma})_j}{\sigma_j} \right)^2 = (b - y)^T\mathbf{W}(b - y) = b^T\mathbf{W}b - 2b^T\mathbf{W}y + y^T\mathbf{W}y, \quad [14]$$

where $\vec{\gamma}$, σ, b and y are, vector of N parameters, measurement errors, experimental (or synthetic) data and simulated data obtained by some arbitrary taken mathematical model (i.e., $y = Y(\vec{\gamma})$). $\mathbf{W}$ is the weighting diagonal matrix with elements equal to 1 (i.e., $W_{j,j} = 1/\sigma_j = 1$). Although $\mathbf{W}$ is the identity matrix in this work, we still use it in 14 for the sake of generality, since in our previous DRT study[6] we applied $\mathbf{W}$ with elements different to 1.

However, in LMA, the minimization is conducted by iterations; and thus, in each iteration it is required to determine perturbation $\vec{\delta}$ to the parameters $\vec{\gamma}$ that reduces 14. The model Y in 14 with perturbed parameters can be locally approximated by using the Taylor series expansion (see, e.g., Ref. 33):

$$Y(\vec{\gamma} + \vec{\delta}) \approx Y(\vec{\gamma}) + \frac{\partial Y}{\partial \vec{\gamma}}\vec{\delta} = Y(\vec{\gamma}) + \mathbf{J}\vec{\delta} = y + \mathbf{J}\vec{\delta}, \quad [15]$$

where $\mathbf{J}$ is the Jacobian matrix. Consequently, 14 can be rewritten as:[22,23]

$$\begin{aligned} S(\vec{\gamma} + \vec{\delta}) &= (b - y - \mathbf{J}\vec{\delta})^T\mathbf{W}(b - y - \mathbf{J}\vec{\delta}) = \\ &= b^T\mathbf{W}b - b^T\mathbf{W}y - b^T\mathbf{W}\mathbf{J}\vec{\delta} - y^T\mathbf{W}b \\ &\quad + y^T\mathbf{W}y + y^T\mathbf{W}\mathbf{J}\vec{\delta} - (\mathbf{J}\vec{\delta})^T\mathbf{W}b \\ &\quad + (\mathbf{J}\vec{\delta})^T\mathbf{W}y + (\mathbf{J}\vec{\delta})^T\mathbf{W}\mathbf{J}\vec{\delta}. \end{aligned} \quad [16]$$

Afterward, the parameter update $\vec{\delta}$ that minimizes $S(\vec{\gamma})$ 14 can be found by setting $\partial S/\partial\vec{\delta} = 0$; and thus, we can write:

$$\begin{aligned} \frac{\partial S(\vec{\gamma} + \vec{\delta})}{\partial \vec{\delta}} &= -b^T\mathbf{W}\mathbf{J} + y^T\mathbf{W}\mathbf{J} - \mathbf{J}^T\mathbf{W}b \\ &\quad + \mathbf{J}^T\mathbf{W}y + 2\mathbf{J}^T\mathbf{W}\mathbf{J}\vec{\delta} \\ &= -2\mathbf{J}^T\mathbf{W}b + 2\mathbf{J}^T\mathbf{W}y + 2\mathbf{J}^T\mathbf{W}\mathbf{J}\vec{\delta} \\ &= -2\mathbf{J}^T\mathbf{W}(b - y) + 2\mathbf{J}^T\mathbf{W}\mathbf{J}\vec{\delta} = 0, \end{aligned} \quad [17]$$

which represents the Gauss-Newton update:

$$(\mathbf{J}^T\mathbf{W}\mathbf{J})\vec{\delta} = \mathbf{J}^T\mathbf{W}(b - y). \quad [18]$$

In the case of the original LMA,[34,35] increment $\vec{\delta}$ is computed from:

$$(\mathbf{J}^T\mathbf{W}\mathbf{J} + \lambda diag(\mathbf{J}^T\mathbf{W}\mathbf{J}))\vec{\delta} = \mathbf{J}^T\mathbf{W}(b - y), \quad [19]$$

where λ is the damping parameter. In this work, $\mathbf{W}$ and $\mathbf{J}$ are the diagonal weighting $2N \times 2N$ matrix ($W_{j,j} = 1$) and the Jacobian $\begin{bmatrix} \mathbf{Z}^{Re} \\ \mathbf{Z}^{Im} \end{bmatrix}$ matrix with $2N \times N + 2$ dimensions.

During the LMA iterations, λ is automatically updated by one of the available update strategies, e.g., Refs. 36, 30, 23, 35. These references are examples of the λ posteriori update strategies that should be generally used when regularizing ill-posed problems.[37] For small λ values, LMA acts like Gauss-Newton method which enables a fast convergence when close to the final solution.[22] Oppositely, for greater λ values LMA mimics the steepest descent method which ensures a short step in the descent direction.[22] The ability of LMA to automatically tune and adapt the λ parameter is crucial in this work as the DRT deconvolution is known to be an inverse ill-posed problem.

DRT extraction setup.—Herein, we have applied the following quadratic objective function proposed by Sheppard et al.[38] to extract DRT from the EIS data:

$$S_{Shepp}(\vec{\gamma}) = \sum_{j=1}^{N} (W_{j,j}[Re(\vec{Z}_{data,j}) - Re(Z_{model,j})]^2 + W_{j,j}[Im(\vec{Z}_{data,j}) - Im(Z_{model,j})]^2), \quad [20]$$

the formulation which has been continuously used in numerous EIS studies[39–42] to solve complex non linear least squares (CNLS) problems.

As in our previously reported strategies[2,6,40,41] both the experimental data and the data generated by a model are stored in $2N \times 1$ columns:

$$\begin{bmatrix} Re(\vec{Z}_{data,1}) \\ \vdots \\ Re(\vec{Z}_{data,N}) \\ Im(\vec{Z}_{data,1}) \\ \vdots \\ Im(\vec{Z}_{data,N}) \end{bmatrix} \text{and} \begin{bmatrix} Re(\vec{Z}_{model,1}) \\ \vdots \\ Re(\vec{Z}_{model,N}) \\ Im(\vec{Z}_{model,1}) \\ \vdots \\ Im(\vec{Z}_{model,N}) \end{bmatrix}, \quad [21]$$

which simplifies the computation task(s) in this work.

If the data arrangement 21 is taken into account, then 20 is identical to 14; and thus, the objective function in this work 20 can be expressed in the matrix notation:

$$S_{Shepp} = \vec{r}^{\,T}\mathbf{W}\vec{r}, \quad [22]$$

where $\vec{r} = b - y$ is the residual.

Please be notified that one can make different data stacking (see, 21) with an intention to simply add a piece of additional information to the objective function 20 as presented in, e.g., Ref. 43. This clearly instructs us how LMA can be easily modified with the decoration of both the input data and the Jacobian matrix (see, Ref. 43).

Iteration procedure.—LMA is an iterative algorithm; an thus, in each $l^{th} + 1$ iteration, the calculated $\vec{\delta}$ increment is added to $\vec{\gamma}_l$ from the previous l^{th} (or starting) iteration:

$$\vec{\gamma}_{l+1} = \vec{\gamma}_l + \vec{\delta}, \quad [23]$$

where the elements of the starting $\vec{\gamma}_1$ vector are arbitrarily taken as 1. The $\vec{\gamma}$ update 23 can be additionally adjusted to avoid negative and non-physical DRT values as demonstrated in Ref. 6:

$$\vec{\gamma}_{l+1} \rightarrow \max\{0, \vec{\gamma}_{l+1}\}. \quad [24]$$

Although one can avoid negative values by using Python library based on "trust region" concept (e.g., Ref. 44), this concept might not be suitable for solving problems consisting of many variables.

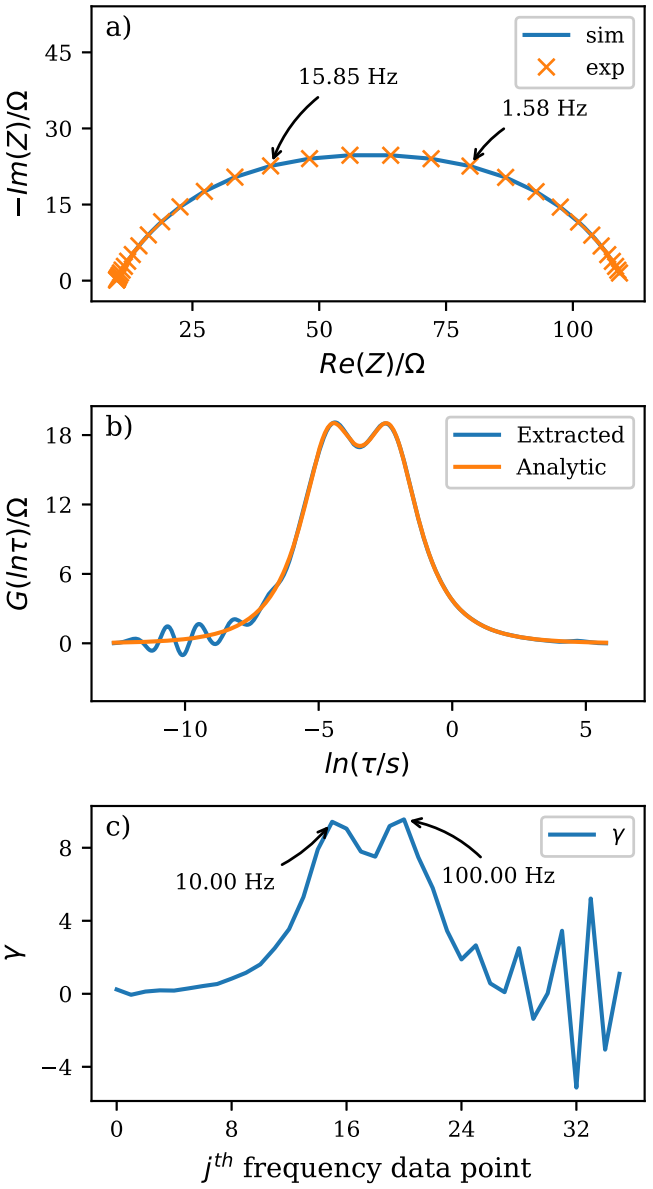

Figure 1. Analysis of (a) complex non-polluted ZARC data. DRT_{ZARCs} (b) data were obtained by using Levenberg-Marquardt algorithm to find the optimal $\vec{\gamma}$ values (c) without the application of both smoothing operator and limits.

This kind of transformation 24 can be used when the Jacobian matrix is available, as in the case of the linear model 13. In other cases, the Jacobian matrix is usually computed in each iteration;[42] and thus, it is necessary to have a continuous objective function S (Scheme 3). The continuous objective function is essential for the computation of the first derivatives; and thus, the application of 24 could hinder the LMA convergence process when solving, e.g., complex nonlinear square (CNLS) problems. Having said that, in strategies reported by Boukamp et al.,[39] the author successfully applied both analytical first derivative expressions and 24 to solve CNLS problem(s). In general, the extraction of $\vec{\gamma}$ by LMA in this work is (almost) identical to the procedure for solving CNLS (see, e.g., Refs. 39–41).

Application of smoothing operator.—When handling the ill-posed inverse problem(s),[1] one is supposed to additionally regularize the problem(s). In this work, the regularization has already been done to some extent by using the damping parameter λ in 19.

However, this self-adapting λ[23] parameter does not have an impact on "smoothness" of the final $\vec{\gamma}$ values 23, 24. According to Ref. 45, LMA can be modified to prevent the oscillations in $\vec{\gamma}$; and consequently in DRT, by minimizing the high-order differences. To be specific, in order to avoid oscillation in $\vec{\gamma}$ values, we need to additionally regularize the problem 19 by using, e.g., finite difference $2N \times 2N$ matrix (see, Refs. 45, 46):

$$\mathbf{Q} = \begin{bmatrix} -2 & 1 & & & & & \\ 1 & -2 & 1 & & & & \\ 0 & 1 & -2 & & & & \\ & & \ddots & \ddots & & & \\ & 0 & & 1 & -2 & 1 & \\ & & & & 1 & -2 & \end{bmatrix}. \qquad [25]$$

The regularization operator ($\mathbf{Q}$) of the form 25 is often addressed as a smoothing operator.[46] Matrix Q corresponds to the use of the second derivative in the penalty term of Tikhonov regularization functional, where the above derivative is approximated by central difference formula (Table I). The numbers 1, −2, 1 in 25 are the coefficients of the Second-order central difference formula approximating the second derivative. Furthermore, $\mathbf{Q}$ matrix 25 is a sparse matrix with nonzero elements on the main diagonal and on the diagonals below and above. This matrix is a tridiagonal[47] matrix, which is also used as a regularization matrix in the Tikhonov regularization of some discrete ill-posed problems.[46]

If we want to obtain smooth $\vec{\gamma}$ values then according to Ref. 45, 19 should be modified:

$$(\mathbf{J}^T\mathbf{W}\mathbf{J} + \lambda\mathbf{Q}^T\mathbf{Q})\vec{\delta} = \mathbf{J}^T\mathbf{W}(b - y), \qquad [26]$$

where the regularization (hyper)parameter λ appears as a multiplication factor near the penalty term defined by Q matrix. The application of 26 is an attempt to bring this DRT study beyond the one previously published by our group.[6] Moreover, the formulation 26 further promotes the original LMA regularization idea initially advocated in Refs. 34, 35. The LMA iteration procedures that yield both positive and smooth DRT values 24, 26 are listed in Algorithm 1.

---

begin
$l := 1$; $\vec{\gamma} := \vec{\gamma}_1$; $\vec{r} = \vec{Z}_{data} - \vec{Z}_{model}(\gamma)$; $\lambda := \lambda_1$
found $:= \|\mathbf{J}^T\mathbf{W}\vec{r}\|_\infty \leqslant \epsilon_1$
while (*not found*) *and* $(l < l_{\max})$ $\quad l := l + 1$;
Solve$(\mathbf{J}^T\mathbf{W}\mathbf{J} + \lambda\text{diag}(\mathbf{J}^T\mathbf{W}\mathbf{J}))\vec{\delta} = \mathbf{J}^T\mathbf{W}\vec{r}$
(in the case of smoothing: Solve$(\mathbf{J}^T\mathbf{W}\mathbf{J} + \lambda(\mathbf{Q}^T\mathbf{Q}))\vec{\delta} = \mathbf{J}^T\mathbf{W}\vec{r}$
if $\|\vec{\delta}\| \leqslant \epsilon_2(\|\vec{\delta}\| + \epsilon_2)$
found $:=$**true**

else
$\vec{\gamma}_{new} := \vec{\gamma} + \vec{\delta}$
(in the case of limits: $\vec{\gamma}_{new} \rightarrow \max\{0, \vec{\gamma} + \vec{\delta}\}$)
$\vec{r}_{new} = \vec{Z}_{data} - \vec{Z}_{model}(\gamma_{new})$
$\rho := \vec{r}^{\,T}\mathbf{W}\vec{r} - \vec{r}^{\,T}_{new}\mathbf{W}\vec{r}_{new}$
if $\rho > 0$ **then**
$\vec{\gamma} := \vec{\gamma}_{new}$
$\vec{r} = \vec{Z}_{data} - \vec{Z}_{model}(\gamma)$
found $:= \|\mathbf{J}^T\mathbf{W}\vec{r}\|_\infty \leqslant \epsilon_1$
$\lambda = \lambda/2$
else
$\lambda = \lambda \cdot 3$
end
end
end

The above formulation 26, as reported in Ref. 45 prevents an extensive oscillation in $\Delta\vec{\gamma}$. The same smoothing effect obtained by the smoothing operator 25 was also reported in Ref. 46. Although it should be stressed that there are various finite difference matrices that can be used as smoothing operators.[48,46] Interestingly, a similar trick, i.e., the stabilization of DRT data by the application of the Toeplitz matrix, was also used by Wan et al.[3] (Table I).

Algorithm 1.Levenberg-Marquardt algorithm applied to 19. $\mathbf{J}$ and $\mathbf{W}$ matrices are not updated during the loop. λ_1, $\epsilon_1$andϵ_2 are (small) values chosen by the user and $\vec{r}$ is the data residual vector.

Comparison of DRT methods of keen interest.—An automatic tuning of the regularization parameter (via LMA) is one of the advantages of our new DRT approach. Moreover, adding one more algorithm to the arsenal of methods for extracting DRT (e.g., Refs. 2–4,6) is worth of doing, because at the top of that arsenal (Table II) one can implement the aggregation procedure in the same way as it is described in our previous paper.[2] Then, the more algorithms from the above arsenal are employed, the more reliable will be the final approximation of DRT resulted from their aggregation. Furthermore, in Ref. 6 the regularization parameter is automatically tuned by LMA, but this approach also yields oscillations and negative DRT values. On the other hand, the proposed method results in positive values and the bell-shaped DRT profile and in the same time it automatically tunes the regularization parameter which is an improvement when compared to other methods in Table II.

Experimental

Synthetic ZARCs and FRACs impedance data preparation.—In this study, we used Cole-Cole (ZARC)[50] and Davison-Cole (FRAC)[51] models to generate synthetic EIS data. The similarities between these two models are explained in Barsoukov et al.[52] and in our previous work,[6] i.e., both models act as semi-circles at the low frequencies. The data from the aforementioned models are available at no cost; and thus, they are frequently used for testing different optimization algorithms and various Distribution Function of Relaxation Time (DRT) strategies.

The following formulation was applied to prepare synthetic ZARCs ($k = 2$) impedance data that are widely used in DRT studies:[2,3,8]

$$Z_{ZARC}(\omega_j) = R_\infty + \sum_{k=1}^{k=K} \frac{R_k}{1 + (i\omega_j\tau_{0,k})^{n_k}}, \quad k = 1, 2, \ldots, K, \qquad [27]$$

where ω is angular frequency, i is the imaginary unit, R_k is the resistance, n_k is parameter related to constant phase element, $\tau_{0,k}$ is the time constant and R_∞ the high-frequency cutoff resistance.

Furthermore, to conduct a more comprehensive study, researchers can also apply synthetic FRACs ($k = 2$) impedance data:

$$Z_{FRAC}(\omega_j) = R_\infty + \sum_{k=1}^{k=K} \frac{R_k}{(1 + i\omega_j\tau_{0,k})^{n_k}}, \quad k = 1, 2, \ldots, K. \qquad [28]$$

The FRAC impedance data are especially interesting as their analytical DRT profile is hard to mimic due to existence of discontinuities. Additionally, since DRT extraction is sensitive to noise,[2,6,7] the synthetic ZARCs and FRACs impedance data can be polluted by noise:

$$Z_{poll}(\omega_j) = Z_{ZARCs}(\omega_j)(1 + NF(\eta_j' + i\eta_j'')), \qquad [29]$$

Table I. Properties of LMA and RNTM optimization techniques applied in the DRT study. The new strategy differs from the original LMA due to application of limits and smoothing operator.

Properties	LMA		RNTM
	original "damped"[34,35]	new strategy	"trust region"[49]
limits	no	yes	yes
smoothing operator	no	yes (see, Ref. 45)	yes (see, Ref. 3)
additional subproblem	no	no	yes

Table II. Comparison of the regularization DRT methods of keen interest.

DRT method	regularization parameter choice	stabilizer/smoothing matrix	bell-shaped profile
Gavrilyuk et al.[4]	manual	yes	yes
Wan et al.[3]	manual	yes	yes
Žic et al.[2,6]	automatic	no	no
new method	automatic	yes	yes

Table III. Parameters used to compute ZARCs and FRACs data.

Synthetic data	$R_\infty(\Omega)$	$R_1(\Omega)$	$\tau_{0,1}$(s)	n_1	$R_2(\Omega)$	$\tau_{0,2}$(s)	n_2
ZARCs/FRACs	10	50	0.1	0.7	50	0.01	0.7

where NF is the noise factor (i.e., 0.001) and η' and η'' are normally distributed random variables with zero mean and variance one. This approach was also used in different DRT studies.[3,6]

The frequency data points were chosen from the following interval: 0.01 to 100 kHz, by selecting 36 (5 points per decade) frequency data points. The parameters utilized to compute complex ZARCs and FRACs data are given in Table III.

Analytic DRT data preparation.—ZARC and FRAC impedance data are particularly appropriate for DRT studies as their analytical DRT data are known (see, e.g., Refs. 8, 3):

$$g(\tau)_{ZARC} = \sum_{k=1}^{k=K} \frac{R_k}{2\pi\tau} \times \frac{\sin((1-n_k)\pi)}{\cosh(n_k ln(\frac{\tau}{\tau_{0,k}}) - \cos((1-n_k)\pi)}, \quad k = 1, 2, \ldots, K, \qquad [30]$$

$$g(\tau)_{FRAC} = \sum_{k=1}^{k=K} \begin{cases} \frac{R_k}{\tau\pi} \frac{\sin(n_k\pi)}{\tau^{-n_k}(\tau_{0,k}-\tau)^{n_k}}, & \text{if } \tau < \tau_0 \\ 0, & \text{if } \tau > \tau_0 \end{cases}, \quad k = 1, 2, \ldots, K. \qquad [31]$$

The application of analytical DRT relations of ZARCs and FRACs ($k = 2$) elements offers an opportunity to test and justify newly developed DRT strategies. Please note that DRT_{FRAC} (31) has discontinuity(ies), i.e., DRT_{FRAC} values are increasing as $\tau \to \tau_0$, while for $\tau > \tau_0$ DRT_{FRAC} takes 0 value. This sudden change (i.e., discontinuity) in DRT_{FRAC} is generally hard to mimic by available DRT methods (see, e.g., Refs. 2, 3, 6, 8).

Software tools.—In this study, the open-source Python programming language (3.7.4) was used. NumPy[53] was applied for the computation tasks, SciPy was utilized for numerical integration,[25] while Matplotlib[54] was employed for the presentation of the results.

Results and Discussion

Analysis of* non-polluted *ZARCs and FRACs data.—Herein, non-polluted ZARCs (Fig. 1a) and FRACs (Fig. 2a) data were analyzed by the proposed strategy (see Scheme 1). These DRT profiles were extracted by using Levenberg-Marquardt algorithm, i.e., by using 19. The extraction procedure was carried out without both the limits and the smoothing operator, which is a common practice for LMA.[41] According to Fig. 1a and Fig. 2a the simulated ZARCs and FRACs data match well with the experimental EIS data.

Furthermore, the extracted DRT_{ZARCs} and DRT_{FRACs} profiles (Fig. 1b and Fig. 2b) agree well to their analytical DRT counterparts. However, both DRT_{ZARCs} and DRT_{FRACs} data show oscillations that are especially perceived in the case of FRACs data due to the presence of two discontinuities (31). RBF is the symmetrical and continuous curve with the center in τ_m (see Scheme 2); and thus, it is hard to mimic DRT_{FRACs} at $\tau > \tau_0$. Be aware that oscillations in DRT_{FRACs} data are frequently observed in the literature.[2,6,8] Overall, in this specific exercise, the position and height of the extracted (vs analytical) DRT data match well (Fig. 1b and Fig. 2b).

The final $\vec{\gamma}$ values, used to construct DRT by 6, obtained from analyses of non-polluted ZARCs and FRACs data are given in Fig. 1c and Fig. 2c. The $\vec{\gamma}$ profile in Fig. 1c is similar to the DRT_{ZARCs} profile. This can be assigned to the application of RBF basis functions (Scheme 2b and 6). However, at higher frequency values, $\vec{\gamma}$ shows significant oscillations that perturbed extracted (vs analytical) DRT_{ZARCs} data (Fig. 1b). In contrast, the $\vec{\gamma}$ values (Fig. 2c) obtained from the FRACs data analysis show more oscillations that induced higher perturbations in the DRT_{FRACs} data (Fig. 2b). The fluctuations in Fig. 1c and Fig. 2c take negative values, but their impact on the DRT data (Fig. 1c and Fig. 2c) was not significant due to the application of RBF 6. This clearly shows that the level of regularization in DRT study has to be carefully tuned as its impact on the final DRT is substantial.

Analysis of* polluted *ZARCs data.—The proposed strategy was put to test by analyzing polluted ZARC data. According to Fig. 3a, the strategy yielded a perfect match between the simulated and experimental ZARCs data. However, the extracted DRT_{ZARCs} profile (Fig. 3b) does not match the analytical one. The final $\vec{\gamma}$ values in

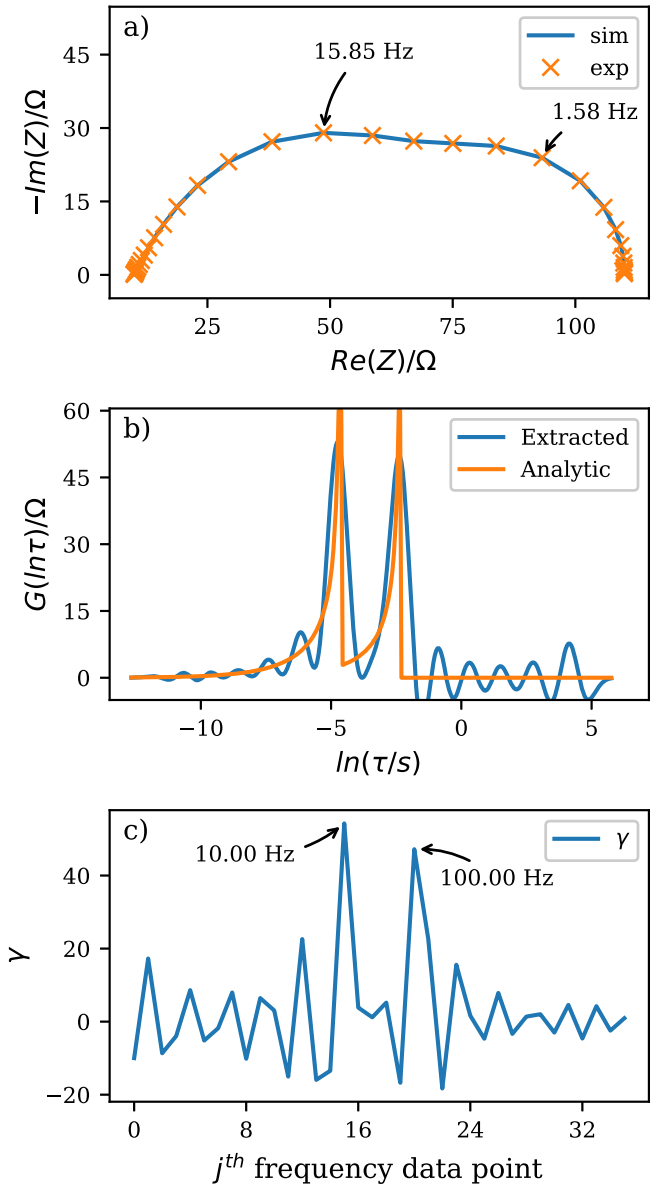

Figure 2. Analysis of (a) complex non-polluted FRACs data. DRT_{FRACs} (b) data were obtained by using Levenberg-Marquardt algorithm to find the optimal $\vec{\gamma}$ values (c) without the application of both smoothing operator and limits.

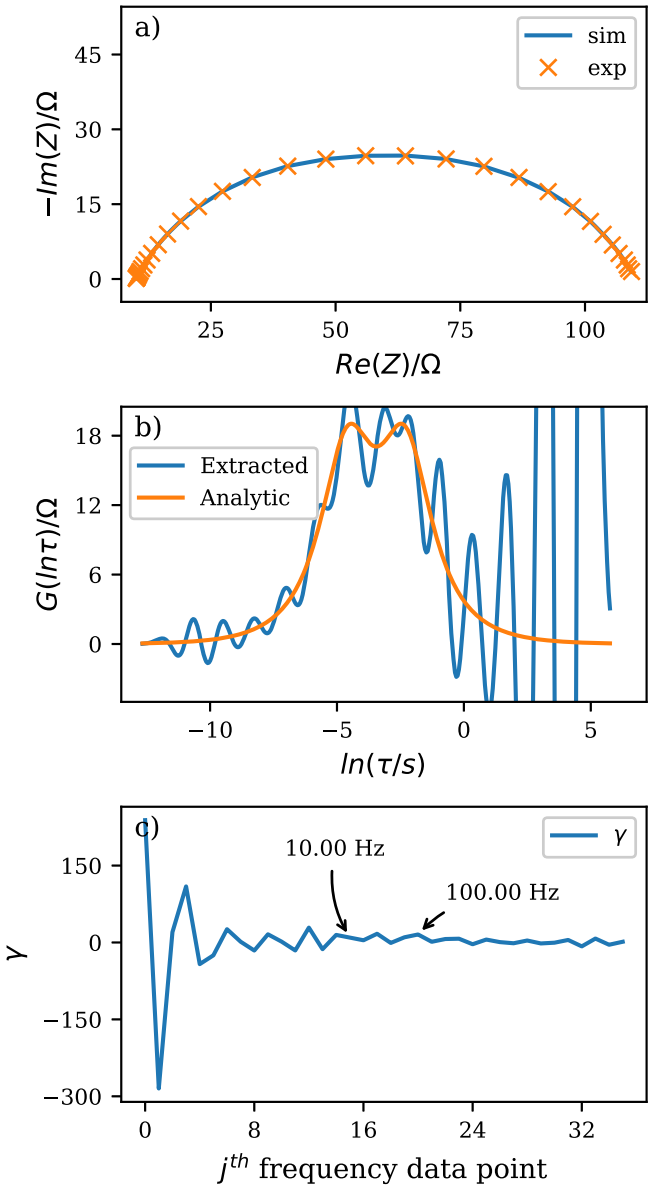

Figure 3. Analysis of (a) complex polluted ZARCs data. DRT_{ZARCs} (b) data were obtained by using Levenberg-Marquardt algorithm to find the optimal $\vec{\gamma}$ values (c) without the application of both smoothing operator and limits.

Fig. 3c also show significant oscillations that consequently induced an inapplicable DRT profile in Fig. 3b. Furthermore, polluted FRACs (vs ZARCs) data produced even more intense DRT_{FRACs} fluctuations promoted by the presence of two discontinuities (FRACs data not shown).

In this paper, several remarks can be stressed. Firstly, the proposed method yielded a firm experimental and simulated data agreement in Fig. 1a, Fig. 2a and Fig. 3a, which indicates that the model 13 was capable of fitting even polluted EIS data. However, the presence of noise induced more severe DRT oscillations (see, Fig. 3b vs Fig. 1b). Secondly, the perfect match in ZARCs data was obtained (Fig. 1a and Fig. 3a) in spite of the fact that $\vec{\gamma}$ data (Fig. 1c and Fig. 3c) were significantly different. This clearly indicates that the DRT extraction is a classic inverse ill-posed problem that has to be attacked by a plethora of different mathematical methods.[1] Third, the oscillations in this study are of greater intensity than in our previous work,[2] an observation that can be also assigned to the numerical approximation of the integral in 12. And finally, the analyzes in the previous sections suggest that the smooth bell-shaped DRT profiles can only be obtained if $\vec{\gamma}$ values (see, e.g., Fig. 1c and Fig. 3c) are positive and smooth.

Application of smoothing operator and limits.—The extraction of $G(ln\ \tau)$ from the integral in 12 is a inverse ill-posed problem; and thus, the regularization has to be applied.[55] For this purpose, we have decided to apply LMA since it has self-adapting regularization (λ) parameter. It was presented that the final $\vec{\gamma}$ values can oscillate (Fig. 3c), which has a direct impact on DRT values (Fig. 3b). Herein, we aim to reduce $\vec{\gamma}$ values fluctuation by the application of limits 24 and the smoothing operator in the form of the **Q** matrix 25.

The data displayed in Fig. 4a again show that experimental and simulated ZARC data match well. Furthermore, in contrast to Fig. 3b, DRT_{ZARCs} data in Fig. 4b agree well with the analytical ones. Such adequate data match can be assigned to a relative smooth and positive $\vec{\gamma}$ data (Fig. 4c vs Fig. 3c) that were obtained due to the application of 26 and 24. Furthermore, the benefits of the automatic tuning of the λ parameter in LMA can be observed by inspecting

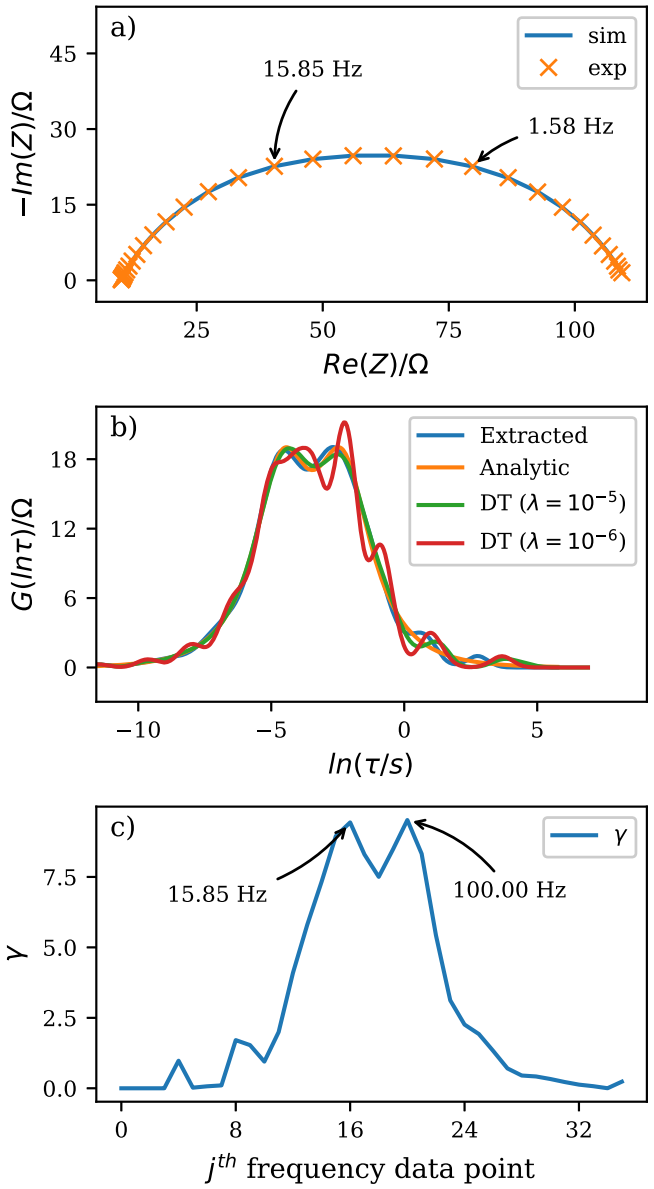

Figure 4. Analysis of (a) complex polluted ZARCs data. DRT_{ZARCs} (b) data were obtained by using Levenberg-Marquardt algorithm to find the optimal γ values (c) by the application of both smoothing operator and limits. DRTtools (DT) data obtained by using two manually selected regularization parameters ($\lambda = 10^{-5}$ and 10^{-6}) are given in (b).

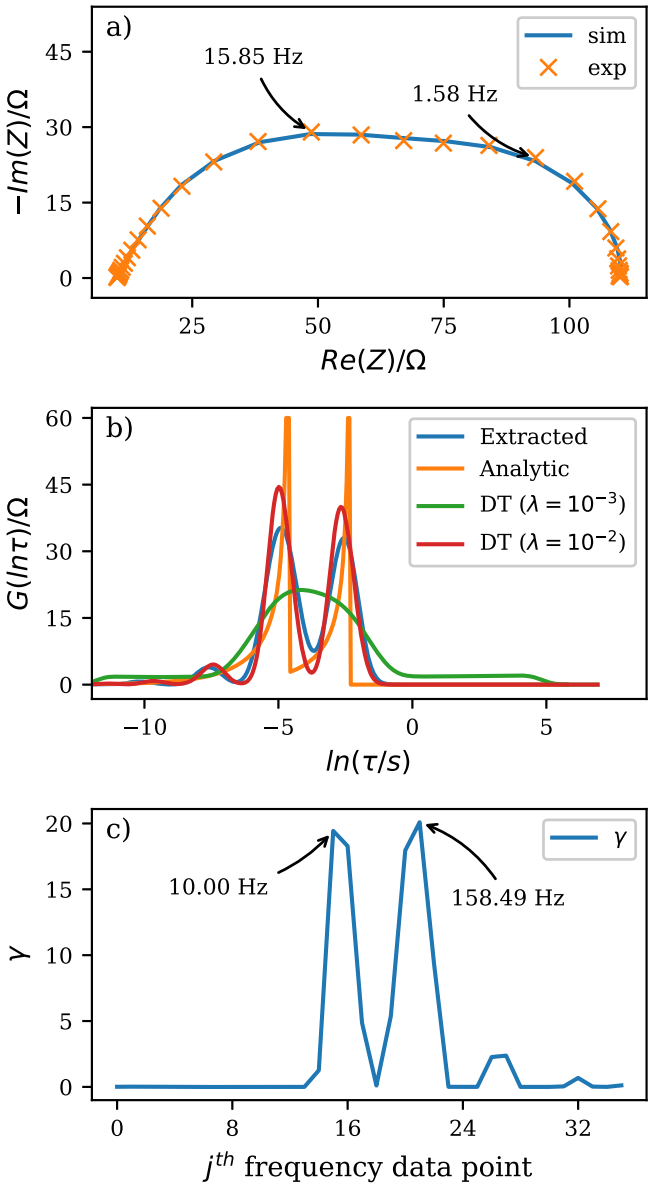

Figure 5. Analysis of (a) complex polluted FRACs data. DRT_{FRACs} (b) data were obtained by using Levenberg-Marquardt algorithm to find the optimal γ values (c) by the application of both smoothing operator and limits. DRTtools (DT) data obtained by using two manually selected regularization parameters ($\lambda = 10^{-2}$ and 10^{-3}) are given in (b).

DRT data obtained by DRTtools (Fig. 4b). The DRT data obtained by manual tuning ($\lambda = 10^{-5}$) in DRTtools agree well with the analytical ones. However, when using $\lambda = 10^{-6}$, which is sufficiently close to manually tuned one ($\lambda = 10^{-5}$), DRT data show several ghost peaks.

Next, to provide more comprehensive analyzes of the impact of the smoothing operator 26, we have analyzed the FRACs data obtained by two FRAC elements (28). These data are of specific interest due to the existence of two discontinuities in DRT spectra (Fig. 5b). Moreover, RBF(s) cannot generally mimic DRT_{FRAC} discontinuities as noted in Ref. 3; and thus, FRACs data are particularly useful for testing purposes. As one can observe, the smoothing of $\vec{\gamma}$ values (Fig. 5c) has yielded an applicable DRT_{FRACs} that match well with the analytical ones (Fig. 5b).

In addition, when using manually tuned $\lambda = 10^{-3}$ value in DRTtools, the DRT_{FRACs} data correspond well with the analytical ones (Fig. 5b). However, when using $\lambda = 10^{-2}$ value only one peak is observed even though Fig. 5a shows the presence of two time constants. The data in Fig. 5b indicates that our new approach does not require visual inspection of EIS data, and at the same time, it is able to automatically choose a proper value of the regularization parameter.

A special interest should be focused on the impact of the $\vec{\gamma}$ transformation 24 on the convergence of the "damping" LMA version.[22] In practice, the application of this transformation perturbs the LMA iteration process, especially if the first derivatives 15 have to be computed.[33] Therefore, the utilization of limits[42] in LMA is rather restricted. However, since the Jacobian matrix in this work is predetermined, the limits 24 can be used (Fig. 5b vs and Fig. 4b), which is a novelty related to the application of the "damped" LMA version[22] in the DRT study. Note that Kulikovsky[7] applied limits 24 by using the "trust region" least squares SciPy library,[56] but the same effect was achieved herein by the utilization of a more elementary "damped" (vs "trust region" reflective algorithm applied in Ref. 7) optimization technique (Scheme 4).

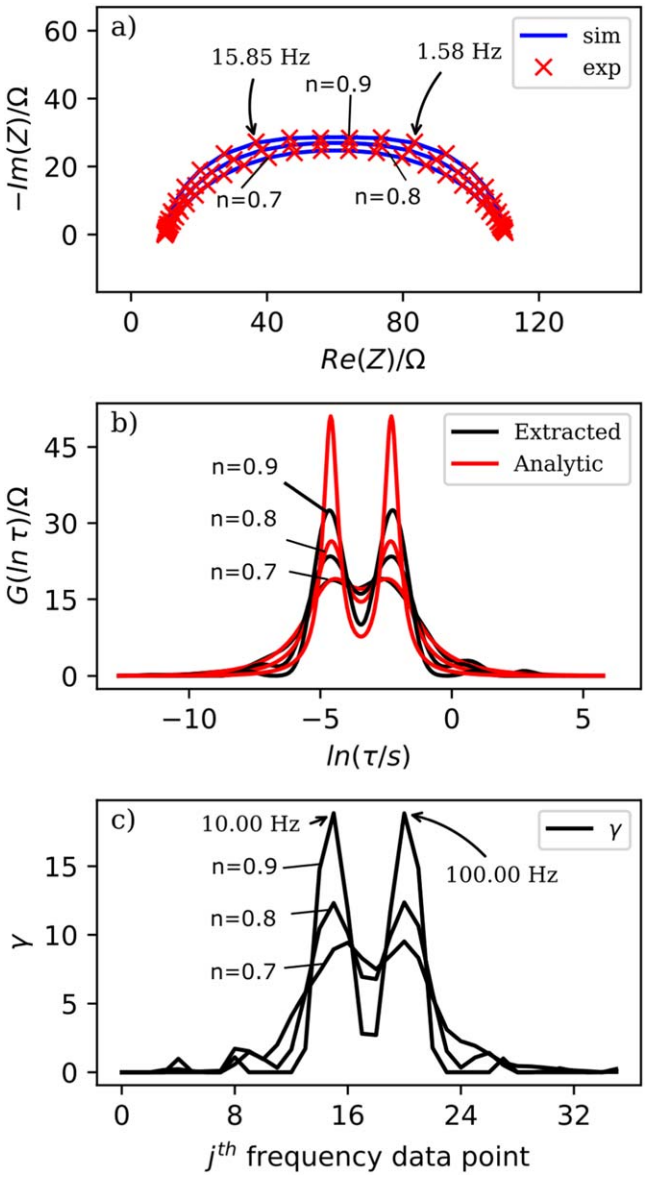

Figure 6. Analysis of (a) different ($n = 0.7$, 0.8 and 0.9) polluted ZARCs data. DRT_{ZARCs} (b) data were obtained by using Levenberg-Marquardt algorithm to find the optimal γ values (c) by the application of both smoothing operator and limits.

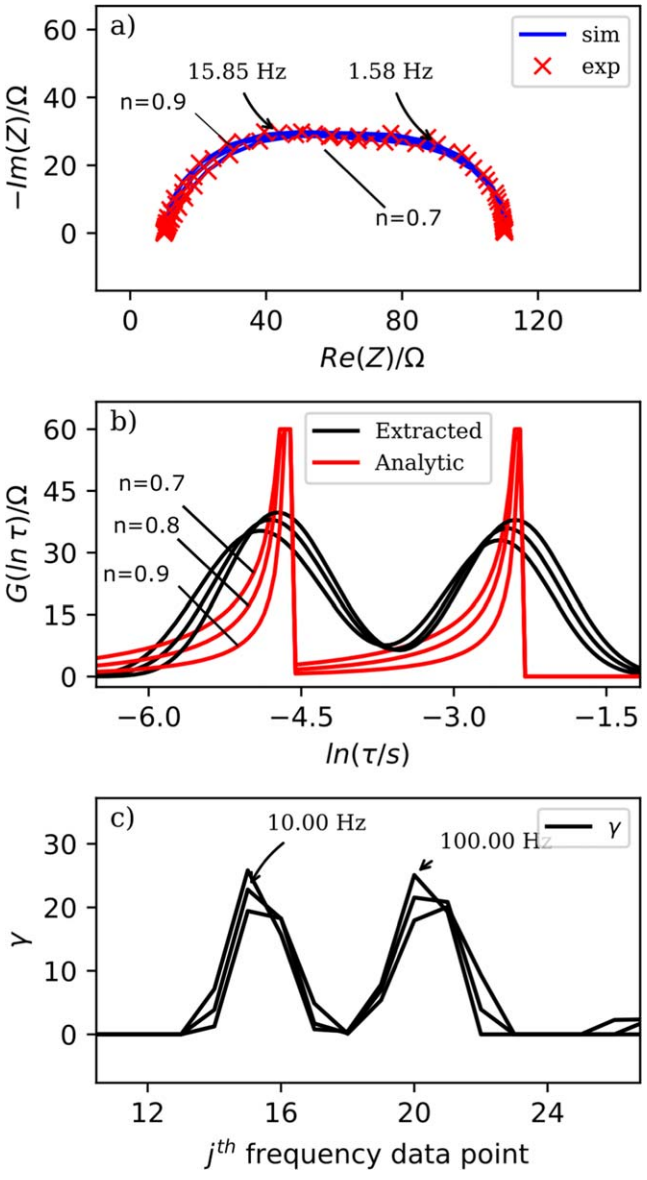

Figure 7. Analysis of (a) different ($n = 0.7$, 0.8 and 0.9) complex polluted FRACs data. DRT_{FRACs} (b) data were obtained by using Levenberg-Marquardt algorithm to find the optimal γ values (c) by the application of both smoothing operator and limits. Subplots (b) and (c) are zoomed, but data related to $n = 0.7$ can be rechecked in Fig. 5b and Fig. 5c.

To summarize, the exercises in this section clearly revealed the benefits of the automatic λ tuning and that it is possible to apply the smoothing operator 25, 26 to decrease the DRT oscillations. What is more, the application of limits 24 dismissed the occurrence of negative and non-physical DRT values (Fig. 5b).

Impact of different* n *values.—Since the synthetic EIS data and their analytic DRT counterpart data are both available at no cost, we have decided to put the impact of different n_k values (27), (28) and (30), (31) on the proposed DRT strategy to the test (Table III). Generally, the value of n has a significant impact on the shape of the depressed semicircle in the complex plain.[52] The same tests were formerly conducted in our previous work.[6] As reported in Fig. 6a, the lower n_k values decreased the maximum of ZARCs depressed semi-circles.

Interestingly enough, the same n_k effect can also be observed in DRT_{ZARCs} curves depicted in Fig. 6b. It appears that the analytic and

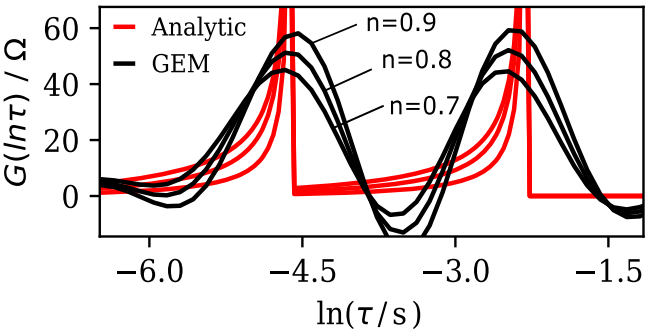

Figure 8. Analysis of different ($n = 0.7$, 0.8 and 0.9) complex polluted FRACs data. DRT_{FRACs} data were obtained by using GEM method, i.e., by using Levenberg-Marquardt algorithm and analytically obtained Jacobian.[6]

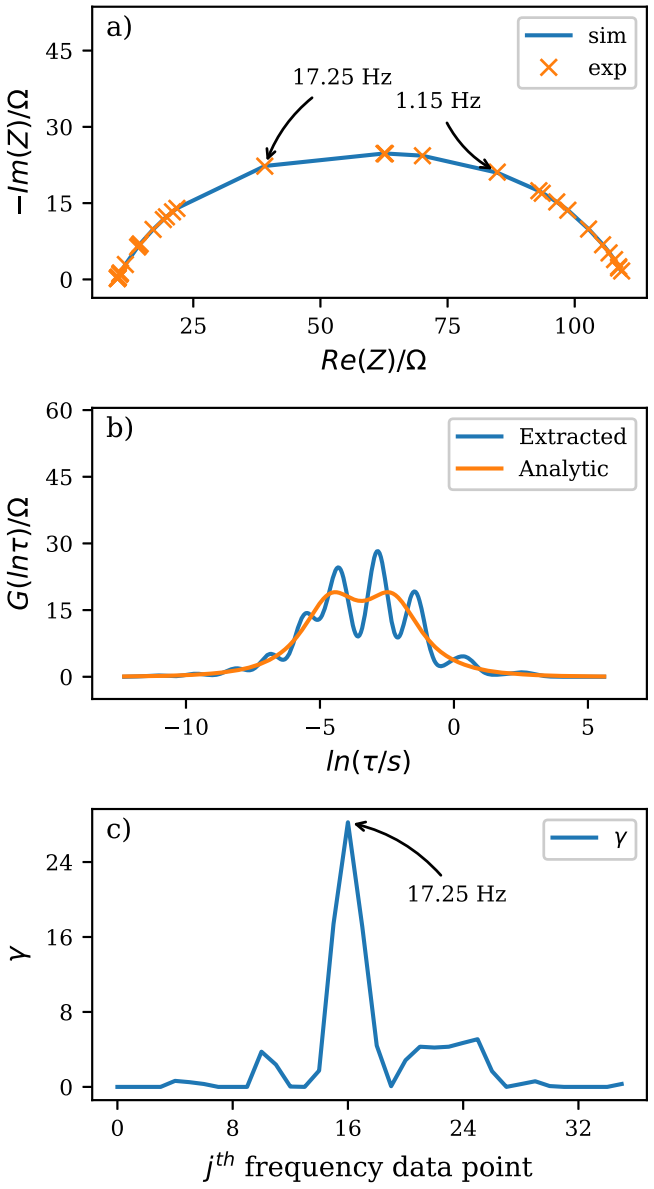

Figure 9. Analysis of (a) complex polluted ZARCs data obtained by using randomly spaced frequency values. DRT_{ZARCs} (b) data were obtained by using Levenberg-Marquardt algorithm to find the optimal γ values (c) by the application of both smoothing operator and limits.

extracted DRT_{ZARCs} peaks match well in the case of $n_k = 0.7$ and 0.8, whilst in the case of $n_k = 0.9$ this resemblance could not be obtained. The data disagreement between analytical and extracted DRT (Fig. 6b) can be assigned to the application of the equal $\epsilon = 0.5$ value 6. Or, put in another way, a better matching might be obtained if the ϵ value is subjected to regularization. However, to automatically tune the ϵ parameter value it is required to design a new DRT strategy, which is a task beyond the scope of this work.

In addition, DRT_{ZARC} is generally smooth and differentiable; and thus, the application of the high-order stabilizers is justified.[4] However, when n is getting closer to 1 (i.e., $n = 0.9$) as in Fig. 6b, DRT becomes the Dirac function which is not smooth and not differentiable. Thus, the application of the high-order Q matrix 25 when n is close to 1 is rather questionable. The experiments with the different n values given in Fig. 6b indicate that the choice of the DRT stabilizer(s) should be further examined.

Further analysis brings additional information obtained by examining several different FRACs data ($n_k = 0.7$, 0.8 and 0.9). As expected, the lowering of n_k value further decreased maxima of depressed FRACs semi-circles (Fig. 7a). In the case of DRT_{FRACs} values, the height of the extracted peaks is gradually being decreased for lower n_k values (Fig. 7b). Also, for the first time in this work, we have observed the shift to the left of the DRT peak maxima. The origin of this shift can be attributed to i) the broadening of DRT_{FRACs} peaks at lower n_k values and ii) the insufficient number of collocation (i.e., $\vec{\gamma}$) points (Fig. 7c) that shape DRT_{FRACs} peaks. Interestingly, the same shift, but of lower intensity, can be observed in Fig. 8 when using the GEM method that applies the analytical solution of the integral in 12.[2] Thus, it is fair to say that the shift of DRT_{FRACs} in Fig. 7b is more intense due to the existence of discretization errors.

Analysis of ZARCs data obtained by using randomly spaced frequency values.—In this specific exercise, carried out by using randomly spaced frequency values, the proposed method produced simulated EIS data that correspond well to the experimental data (Fig. 9a). This is expected as it was demonstrated in previous sections that LMA can fit the EIS data. However, the randomly spaced frequency values hindered DRT deconvolution (Fig. 9b). The extracted DRT data show both oscillations and several ghost peaks that prevent DRT analysis (Fig. 9b). It should be mentioned that this DRT data mismatch indicates the first imperfection of the proposed strategy. To elaborate, according to our previous articles,[2,6] these artificial peaks can be attributed to the discretization errors. Furthermore, GEM method advocated in Refs. 2, 6 showed that it was not perturbed by randomly spaced values since it applies the analytical solution to integral in 2. On the other hand, it should be emphasized that this strategy (vs GEM[6]) yields non-negative and smooth DRT values, which is of great importance for EIS studies.

Future endeavor.—This study clearly presented that the smooth and bell-shaped DRT profile can be obtained by using LMA and the Jacobian matrix, which is partially approximated by applying RBF as a basis for integration. However, we also explained the benefits of DRT study that applies the analytical solution of the integral (see Ref. 6). Therefore, a new strategy should be designed with the intention to exploit all "valid" LMA information gained by using the analytically[6] and numerically (this work) obtained Jacobian matrices. In other words, all trustworthy DRT characteristic (or DRT) values should be aggregated (like in Ref. 2) with an effort to bring top-notch results of the two different DRT methods (i.e., the proposed one and Ref. 6).

Furthermore, herein we demonstrated the impact of the smoothing operator on the DRT data. However, it was stressed in the literature that there are several different smoothing operators.[3,46,45] Thus, their impact on the smoothness of the DFR curve should be additionally investigated.

Conclusions

Herein, we have proposed and designed a new strategy that extracts the Distribution of the Relaxation Times (DRT) from Electrochemical Impedance Spectroscopy (EIS) data by using the Levenberg-Marquardt algorithm (LMA). Unlike the tactics reported in our previous work, this study was focused on the numerical approximation of the DRT integral.

The applicability of the new strategy was tested by applying synthetic ZARCs and FRACs data. The results clearly showed that the new strategy was able to extract the applicable DRT_{ZARCs} and DRT_{FRACs} data profiles.

This venture also demonstrated that LMA can apply the Jacobian matrix, the elements of which consisted mainly of the data obtained by the utilization of the radial basis function (RBF) for the discretization basis. The application of RBF ensured the bell-shaped profile of the extracted DRT data.

The novelty of this work was that LMA was modified to use both the smoothing operator and the limits. The modified LMA induced

rather smooth and non-negative DRT profiles that facilitated the DRT study. This algorithm was able to extract DRT with the same achievement as more complicated quadratic programming techniques.

The presence of the discretization errors in this work (vs[6]) did not perturb LMA convergence process. This clearly indicates that the errors in the Jacobian matrix did not have a significant impact on the solution 26, which can be assigned to regularization obtained by: the λ parameter, the application of the smoothing operator (**Q**), and the RBF employment.

A new DRT approach advocated in this work, was implemented in a new DRT-RBLM v1.01 software, which is shared freely online.[57] The software is capable of analyzing several impedance spectra in batch.

Overall, the outcomes from this study and from our previous work[6] suggest that DRT data from these two strategies should be aggregated.

Acknowledgments

The authors gratefully acknowledge the stimulation program "Incoming Fellowship" (IF-2020) of the Austrian Academy of Sciences. Also, M.Ž. acknowledge Ciucci's Lab for providing their DRTtools code online.

ORCID

M. Žic https://orcid.org/0000-0003-1174-6281

References

1. H. W. Engl, M. Hanke, and A. Neubauer, *Regularization of Inverse Problems* (Springer, Dordrecht, Netherlands) Mathematics and Its Applications, (2000), https://link.springer.com/book/9780792341574.
2. M. Žic, S. J. Pereverzyev, V. Subotić, and S. Pereverzyev, *GEM—International Journal on Geomathematics*, **11**, 2 (2020).
3. T. H. Wan, M. Saccoccio, C. Chen, and F. Ciucci, *Electrochimica Acta*, **184**, 483 (2015).
4. A. L. Gavrilyuk, D. A. Osinkin, and D. I. Bronin, *Russian Journal of Electrochemistry*, **53**, 575 (2017).
5. J. Honerkamp and J. Weese, *Continuum Mechanics and Thermodynamics*, **2**, 17 (1990).
6. M. Žic, L. Vlašić, V. Subotic, S. Pereverzyev, I. Fajfar, and M. Kunaver, *J. Electrochem. Soc.*, **169**, 030508 (2022).
7. A. Kulikovsky, *Physical Chemistry Chemical Physics* (The Royal Society of Chemistry) (2020), ISSN 1463-9084, https://pubs.rsc.org/en/content/articlelanding/2020/cp/d0cp02094j.
8. F. Dion and A. Lasia, *Journal of Electroanalytical Chemistry*, **475**, 28 (1999).
9. K. Kobayashi and T. S. Suzuki, *Electrochemistry*, **90**, 017004 (2022).
10. B. A. Boukamp, *Electrochimica Acta*, **154**, 35 (2015).
11. H. Schichlein, A. C. Muller, M. Voigts, A. Krugel, and E. Ivers-Tiffee, *Journal of Applied Electrochemistry*, **32**, 875 (2002).
12. A. Oz, S. Hershkovitz, N. Belman, E. Tal-Gutelmacher, and Y. Tsur, *Solid State Ionics*, **288**, 311 (2016).
13. S. Hershkovitz, S. Tomer, S. Baltianski, and Y. Tsur, *ECS Trans.*, **33**, 67 (2010).
14. A. B. Tesler, D. R. Lewin, S. Baltianski, and Y. Tsur, *Journal of Electroceramics*, **24**, 245 (2010).
15. M. Kunaver, M. Žic, I. Fajfar, T. Tuma, A. Bűrmen, V. Subotić, and V. Rojec, *Processes*, **9**, 1859 (2021).
16. T. Horlin, *Solid State Ionics*, **107**, 241 (1998).
17. E. Tuncer and J. R. Macdonald, *J. Appl. Phys.*, **99**, 074106 (2006).
18. E. Quattrocchi, T. H. Wan, A. Belotti, D. Kim, S. Pepe, S. V. Kalinin, M. Ahmadi, and F. Ciucci, *Electrochimica Acta*, **392**, 139010 (2021).
19. A. Maradesa, B. Py, E. Quattrocchi, and F. Ciucci, *ChemRxiv* (2021), https://chemrxiv.org/engage/chemrxiv/article-details/61aae175f35d4c5e0950df2a.
20. A. Maradesa, B. Py, E. Quattrocchi, and F. Ciucci, *Electrochimica Acta*, **413**, 140119 (2022).
21. T. F. Coleman and Y. Y. Li, *Siam Journal on Optimization*, **6**, 418 (1996).
22. K Madsen and H B Nielsen, *Introduction to Optimization and Data Fitting* (Informatics and Mathematical Modelling, Technical University of Denmark, DTU), Richard Petersens Plads, Building 321, DK-2800 Kgs. Lyngby) (2010), http://www2.compute.dtu.dk/pubdb/pubs/5938-full.html.
23. H. Nielsen, *Damping Parameter in Marquardt's Method* (1999), Informatics and Mathematical Modelling, Technical University of Denmark, DTU https://www2.imm.dtu.dk/documents/ftp/tr99/tr05_99.pdf.
24. S. Risse, N. A. Cañas, N. Wagner, E. Härk, M. Ballauff, and K. A. Friedrich, *Journal of Power Sources*, **323**, 107 (2016).
25. P. Virtanen et al.(SciPy 10 Contributors), *Nature Methods*, **17**, 261 (2020).
26. J. Wolberg, *Data Analysis Using the Method of Least Squares* (Springer, Berlin, Germany) 2006th ed ed. (2005).
27. L. Landweber, *American Journal of Mathematics*, **73**, 615 (1951).
28. M. R. Hestenes and E. Stiefel, *Methods of Conjugate Gradients for Solving Linear Systems*, **49**, 409 (1952).
29. H. Gavin, (2013)"The Levenberg-Marquardt method for nonlinear least squares curve-fitting problems." http://people.duke.edu/~hpgavin/ce281/lm.pdf.
30. C. Kanzow, N. Yamashita, and T. Fukushima, *Journal of Computational and Applied Mathematics*, **172**, 375 (2004).
31. J. J. Moré, *The Levenberg-Marquardt Algorithm: Implementation and Theory Numerical Analysis* (Springer, Berlin, Heidelberg) p.105 (1978).
32. K. E. J J Moré and B. S. G Hillstrom, *User Guide for MINPACK-1 Tech. rep. Argonne National Laboratory Report ANL-80-74 Argonne* (1980), https://www.osti.gov/biblio/6997568.
33. C. T. Kelley, *Iterative Methods for Optimization* (Society for Industrial and Applied Mathematics, Philadelphia, PA) (1999), Frontiers in applied mathematics.
34. K. Levenberg, *Quarterly of Applied Mathematics*, **2**, 164 (1944).
35. D. W. Marquardt, *Journal of the Society for Industrial and Applied Mathematics*, **11**, 431 (1963).
36. M. Lampton, *Comput. Phys.*, **11**, 110 (1997).
37. S. V. Pereverzev, S. G. Solodky, V. B. Vasylyk, and M. Žic, *Computational Methods in Applied Mathematics*, **20**, 517 (2020), ISSN 1609-4840, 1609-9389 publisher: De Gruyter Section: Computational Methods in Applied Mathematics https://www.degruyter.com/view/journals/cmam/20/3/article-p517.xml.
38. R. J. Sheppard, B. P. Jordan, and E. H. Grant, *Journal of Physics D-Applied Physics*, **3**, 1759 (1970).
39. B. A. Boukamp, *Solid State Ionics*, **20**, 31 (1986).
40. M. Žic, *Journal of Electroanalytical Chemistry*, **760**, 85 (2016).
41. M. Žic, *Journal of Electroanalytical Chemistry*, **799**, 242 (2017).
42. M. Žic, V. Subotić, S. Pereverzyev, and I. Fajfar, *Journal of Electroanalytical Chemistry*, **866**, 114171 (2020).
43. S. Agarwal, K. Mierle, and T. C. S. Team, (2022), Ceres Solver https://github.com/ceres-solver/ceres-solver.
44. M. Newville, T. Stensitzki, D. B. Allen, and A. Ingargiola, (2014), Lmfit: Non-linear least-square minimization and curve-fitting for python, https://doi.org/10.5281/zenodo.11813.
45. L. W. Chan, "Levenberg-Marquardt Learning and Regularization." *Progress in Neural Information Processing*, Hong Kong(Springer) p.139 (1996).
46. L. Reichel and Q. Ye, *ETNA. Electronic Transactions on Numerical Analysis [electronic only]*, **33**, 63 (2008), https://etna.math.kent.edu/vol.33.2008-2009/pp63-83.dir/pp63-83.pdf.
47. S. Noschese, L. Pasquini, and L. Reichel, *Numerical Linear Algebra with Applications*, **20**, 302 (2013).
48. J. Hesse and A. Rubartsch, *J. Phys. E*, **7**, 526 (1974).
49. T. F. Coleman and Y. Li, *SIAM Journal on Optimization*, **6**, 1040 (1996).
50. K. S. Cole and R. H. Cole, *J. Chem. Phys.*, **9**, 341 (1941).
51. D. W. Davidson and R. H. Cole, *The Journal of Chemical Physics*, **19**, 1484 (1951).
52. E. Barsoukov and J. Ross Macdonald, *Impedance Spectroscopy: Theory, Experiment, and Applications, Second Edition* (Wiley, Nashville, TN) 2nd ed. (2005).
53. S. van der Walt, S. C. Colbert, and G. Varoquaux, *Computing in Science & Engineering*, **13**, 22 (2011).
54. J. D. Hunter, *Computing in Science & Engineering*, **9**, 90 (2007).
55. P. Mathe and S. V. Pereverzev, *Inverse Problems*, **19**, 1263 (2003).
56. M. A. Branch, T. F. Coleman, and Y. Li, *SIAM Journal on Scientific Computing*, **21**, 1 (1999).
57. M. Žic, (2022), DRT-RBLM software v.1.01, https://sites.google.com/view/drt-rblm-software/home.